known toxic effects of salt spray on the twigs that grow into the higher-velocity portions of the airstream flowing off the ocean and over the secondary dune (*10*). The growth response of the forest trees simultaneously adapts the ecosystem to the wind-salt conditions and limits further biomass accumulation resulting from upward growth. However, proliferation of branches at the airstream-canopy interface guarantees a large surface area that probably strains aerosols from slower, nontoxic portions of the airstream. Thus, there are continual adjustments between the restriction of the system by toxic effects of salt spray and dependence of the system on salt spray as a source of nutrients.

The rates of development, biomass accumulation, and net primary production approach the means for temperate forests (*5*). Dimension analyses (*17*) indicated a biomass of 17,000 g/m^2, a net primary production of 1110 g/m^2, and a leaf area index of 5.9, all of which fall well within the range for temperate forests. This is in part because nutrients from meteorologic sources alone are about equivalent to nutrients from meteorologic plus weathering sources in a variety of other ecosystems (Table 2).

The development of an ecosystem may be extremely slow if low weathering rates are coupled with low rates of meteorologic input. These factors may be important along Lake Michigan, where fresh water dune ecosystems take thousands of years to reach the tree stage (*18*). Radiocarbon dates and geological evidence suggest that the Sunken Forest has reached a comparable stage of development in only 200 to 300 years (*19*).

Our results also suggest that the high levels of biomass accumulation and primary production found in some coastal regions (*5, 17, 20*), may be in part due to high weathering inputs plus high meteorologic inputs.

HENRY W. ART
Biology Department and Center for Environmental Studies, Williams College, Williamstown, Massachusetts 01267
F. HERBERT BORMANN
GARTH K. VOIGT
School of Forestry and Environmental Studies, Yale University, New Haven, Connecticut 06511
GEORGE M. WOODWELL
Biology Department, Brookhaven National Laboratory, Upton, New York 11973

References and Notes

1. F. H. Bormann and G. Likens, *Science* **155**, 424 (1967).
2. F. W. Clarke, *U.S. Geol. Surv. Bull. 770* (1924); B. Mason, *Principles of Geochemistry* (Wiley, New York, 1966).
3. G. Likens and F. H. Bormann, in *Ecosystem Structure and Function*, J. A. Wiens, Ed. (Oregon State Univ. Press, Corvalis, 1972), pp. 25–67.
4. G. M. Woodwell and R. H. Whittaker, in *Symposium on Primary Productivity and Mineral Cycling in Natural Ecosystems*, H. E. Young, Ed. (Univ. of Maine Press, Orono, 1967), p. 151.
5. H. W. Art, thesis, Yale University (1971).
6. F. Cowan, personal communication. Cowan also reported the complete absence of feldspars and micas in a mineralogical analysis of soils from the Sunken Forest.
7. H. C. Crandell, *U.S. Geol. Surv. Water Supply Pap. 1539-X* (1962).
8. W. B. Harris, *Water Resour. Res.* **3**, 89 (1967).
9. R. H. Whittaker, *Ecology* **42**, 171 (1961); *ibid.* **43**, 357 (1962); *ibid.* **44**, 176 (1963); *ibid.* **46**, 365 (1965); *ibid.* **47**, 103 (1966); ——— and G. M. Woodwell, *Am. J. Bot.* **54**, 931 (1967); *J. Ecol.* **56**, 1 (1968); *ibid.* **57**, 155 (1968); G. Likens and F. H. Bormann, *Yale Univ. Sch. For. Bull. 79* (1970); ———, N. M. Johnson, R. S. Pierce, *Ecology* **48**, 772 (1967). Cation analysis was performed by atomic absorption spectrophotometry.
10. S. G. Boyce, *Ecol. Monogr.* **24**, 29 (1954).
11. E. Eriksson, *Tellus* **7**, 243 (1955); F. H. T. Juang and N. M. Johnson, *J. Geophys. Res.* **72**, 5641 (1967); E. J. Conway, *Proc. R. Ir. Acad. Sect. B* **48**, 119 (1942).
12. R. B. Miller, *N.Z. J. Sci.* **6**, 388 (1963).
13. The relation between kilograms Na impacted per hectare (Y) and thousands of kilometers of wind blowing onshore (between 79° and 238°) at speeds of <7 (X_1) and >7 (X_2) meter/sec is given by $Y = 2.49X_1 + 3.57X_2 - 0.264$ (multiple correlation coefficient, .84; F value of the regression, 39.4; 2 and 34 degrees of freedom; significant at $P < 0.1$ percent). The amounts of K, Ca, and Mg impacted are calculated by multiplying the amount of Na by the K/Na, Ca/Na, and Mg/Na ratios, 0.0435, 0.0519, and 0.139, respectively.
14. The relation between cation exchange capacity in milliequivalents per 100 g of soil (Y) and organic matter expressed as percentage loss on ignition (X) is given by $Y = 1.51X - 0.24$ (multiple correlation coefficient, .97; F value of the regression, 300.5; 1 and 22 degrees of freedom; significant at $P < 0.1$ percent). The relation between total exchangeable K + Na + Ca + Mg in milligrams per kilogram of soil (Y) and organic matter expressed as percentage loss on ignition (X) is given by $Y = 67.44X - 19.56$ (multiple correlation coefficient, .88; F value of the regression, 72.8; 1 and 22 degrees of freedom; significant at $P < 0.1$ percent).
15. C. O. Tamm, *Physiol. Plant.* **4**, 461 (1951); H. L. Mitchell, *Black Rock For. Pap.* **1** (No. 6), 30 (1936).
16. P. W. Richards, *The Tropical Rain Forest* (Cambridge Univ. Press, Cambridge, 1964); I. Langdale-Brown, in *The Soil Resources of Tropical Africa*, R. P. Moss, Ed. (Cambridge Press, Cambridge, 1968), p. 61.
17. H. W. Art and P. L. Marks, in *Forest Biomass Studies*, H. E. Young, Ed. (Univ. of Maine Press, Orono, 1971), p. 1.
18. H. C. Cowles, *Bot. Gaz.* **27**, 95, 167, 281, 361 (1899); J. S. Olson, *ibid.* **119**, 125 (1958).
19. L. A. Sirkin, *Bull. Torrey Bot. Club.* **94**, 131 (1972).
20. A. T. Wilson, *Nature (Lond.)* **184**, 99 (1959).
21. D. W. Cole, S. P. Gessel, S. F. Dice, in *Symposium on Primary Productivity and Mineral Cycling in Natural Ecosystems*, H. E. Young, Ed. (Univ. of Maine Press, Orono, 1967), p. 198.
22. Supported by the Fire Island National Seashore, National Park Service, Brookhaven National Laboratory, and Yale University. We thank the U.S. Coast Guard, the U.S. Geological Survey, B. Bormann, P. Bernacki, K. K. Turekian, W. Oakley, and T. G. Siccama for assistance during the study, and P. L. Marks for helpful comments on the manuscript.

10 December 1973

Radiohalos in a Radiochronological and Cosmological Perspective

Abstract. *New photographic evidence, data on halo ring sizes, and x-ray fluorescence analyses provide unambiguous evidence that polonium halos exist as a separate and distinct class apart from uranium halos. Because of the short half-lives of the polonium isotopes involved, it is not clear how polonium halos may be explained on the basis of currently accepted cosmological models of Earth formation.*

I have examined some 10^5 or more radiohalos, mainly from Precambrian granites and pegmatites located in several continents. In addition to U and Th halos, originally studied (*1, 2*) for information on the constancy of the α-decay energy E_α and the decay constant λ, I have discussed X halos (*2, 3*), dwarf halos (*3*), and giant halos (*4*), and explained how these remain prime candidates for identifying unknown α-radioactivity and, not impossibly, unknown elements as well.

I have also reported (*5*) on a class of halos which had been tentatively attributed (*6, 7*) to the α-decay of ^{210}Po, ^{214}Po, and ^{218}Po. Earlier investigators (*2, 7–10*), possessing only a sparse collection of Po halos, at times confused them with U halos or invented spurious types such as "emanation" halos (*2*) or "actinium" halos (*8*) to account for them. (Figure 1, a to d, is a schematic comparison of U and Po halo types with ring radii drawn proportional to the respective ranges of α-particles in air.) To explain Po halos, Henderson (*7*) postulated a slow accumulation of Po isotopes (or their respective β-decay precursors) from U daughter product activity. I demonstrated that this secondary accumulation hypothesis was untenable and showed, using the ion microprobe (*3*), that Po halo radiocenters (or inclusions) exhibit anomalously high ^{206}Pb/^{207}Pb isotope ratios which are a necessary consequence of Po α-decay to ^{206}Pb.

Recently, these ion microprobe results have been questioned, Henderson's results misinterpreted, Po halos con-

sidered to be only U halos, and allusions made to the geological difficulties that Po halos would present if they were real (*11*) [see (*12*) for comments].

Admittedly, compared to ordinary Pb types, the Pb isotope ratios of Po halos are unusual, but new ion microprobe analyses have confirmed (*13*) my earlier results (*3*). It is also apparent that Po halos do pose contradictions to currently held views of Earth history.

For example, there is first the problem of how isotopic separation of several Po isotopes [or their β-decay precursors (*13*)] could have occurred naturally. Second, a straightforward explanation of ^{218}Po halos implies that the 1-μm radiocenters of very dark halos of this type initially contained as many as 5×10^9 atoms (a concentration of more than 50 percent) of the isotope ^{218}Po (half-life, 3 minutes), a problem that almost defies reason. A further necessary consequence, that such Po halos could have formed only if the host rocks underwent a rapid crystallization, renders exceedingly difficult, in my estimation, the prospect of explaining these halos by physical laws as presently understood. In brief, Po halos are an enigma, and their ring structure as well as other distinguishing characteristics need to be made abundantly clear.

In order to ascertain the E_α corresponding to a specific halo radius, I have produced a new series of standard sizes against which halo radii may be compared without relying on estimates derived from ranges of α-particles in air. Standard sizes may be prepared by irradiation of halo-bearing mineral samples with ^{4}He ions (*4*); the coloration bands thus produced show varying sizes (as measured from edge to coloration extinction) which are dependent on energy, total dose, and dose rate, the latter two factors not being accounted for in other comparative methods.

I made more than 350 irradiations 1 to 10^4 seconds in duration using ^{4}He ions with energies ranging from 1 to 15 Mev, on over 40 samples of biotite, fluorite, and cordierite (*14*). Selecting the band sizes which correspond to the energies of the ^{238}U α-emitters (see Table 1) permits a direct comparison with new as well as previous (*1, 9, 10, 15*) U halo measurements in biotite, fluorite, and cordierite. Figure 1e shows a coloration band in biotite produced by 7.7-Mev ^{4}He ions, and Fig. 2a shows a densitometer profile of Fig. 1e.

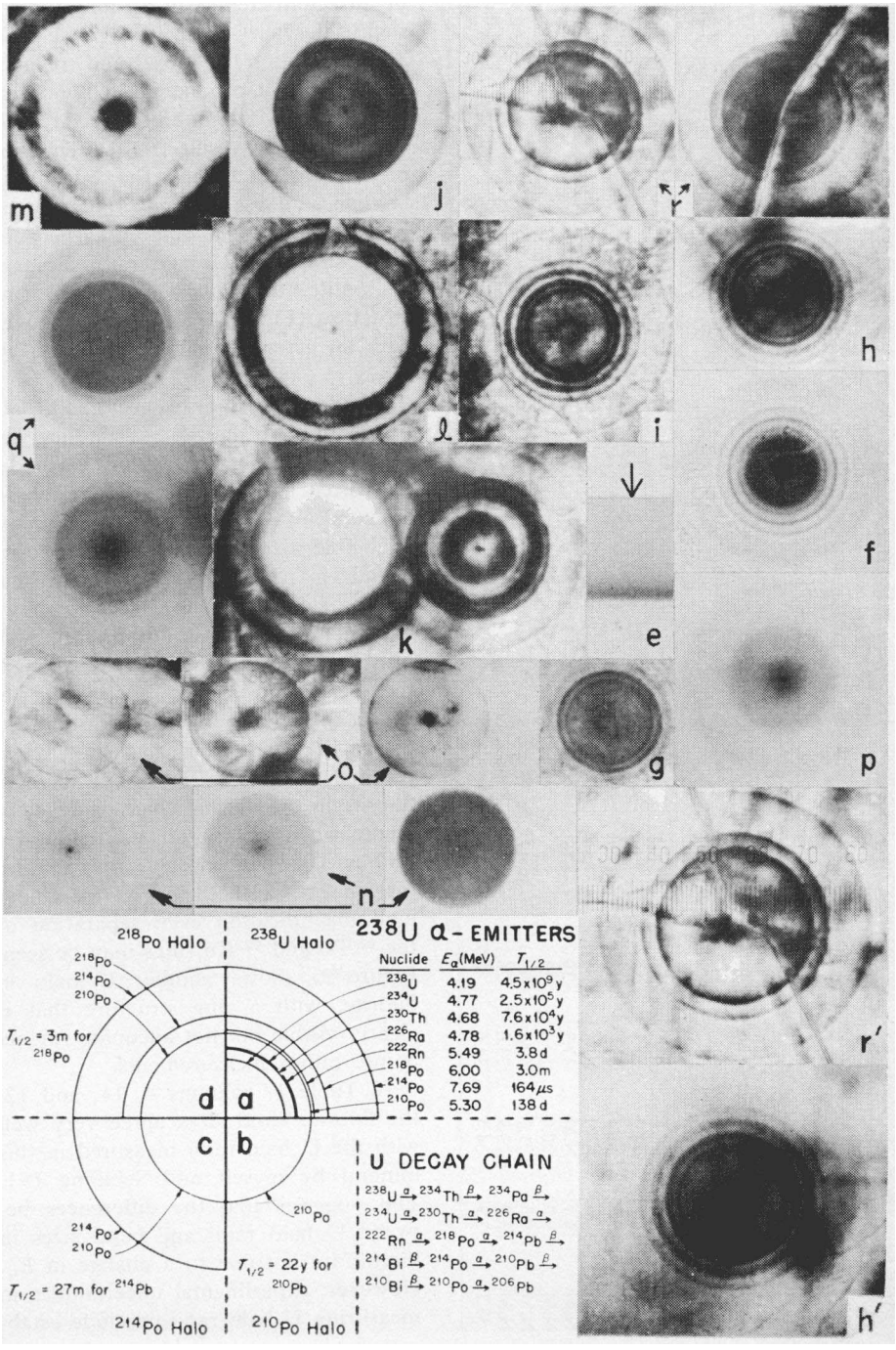

Fig. 1. The scale for all photomicrographs is 1 cm $\simeq$ 25.0 μm, except for (h') and (r'), which are enlargements of (h) and (r). (a) Schematic drawing of ^{238}U halo with radii proportional to ranges of α-particles in air. (b) Schematic of ^{210}Po halo. (c) Schematic of ^{214}Po halo. (d) Schematic of ^{218}Po halo. (e) Coloration band formed in mica by 7.7-Mev ^{4}He ions. Arrow shows direction of beam penetration. (f) A ^{238}U halo in biotite formed by sequential α-decay of the ^{238}U decay series. (g) Embryonic ^{238}U halo in fluorite with only two rings developed. (h) Normally developed ^{238}U halo in fluorite with nearly all rings visible. (h') Same halo as in (h) but at higher magnification. (i) Well-developed ^{238}U halo in fluorite with slightly blurred rings. (j) Overexposed ^{238}U halo in fluorite, showing inner ring diminution. (k) Two overexposed ^{238}U halos in fluorite showing inner ring diminution in one halo and obliteration of inner rings in the other. (l) More overexposed ^{238}U halo in fluorite, showing outer ring reversal effects. (m) Second-stage reversal in a ^{238}U halo in fluorite. The ring sizes are unrelated to ^{238}U α-particle ranges. (n) Three ^{210}Po halos of light, medium, and very dark coloration in biotite. Note the differences in radius. (o) Three ^{210}Po halos of varying degrees of coloration in fluorite. (p) A ^{214}Po halo in biotite. (q) Two ^{218}Po halos in biotite. (r) Two ^{218}Po halos in fluorite. (r') Same halo as in (r) but at higher magnification.

Table 1. Comparison of sizes of induced bands (columns 1 to 5) with halo radii (columns 8 to 21). Column 6 gives the ^{4}He ion energies at which the induced bands were formed, or the α-particle energies corresponding to the nuclides in column 7. Thus, the nuclide or α-particle energy that produced any halo ring in columns 8 to 21 can be found from column 6 or 7. The letters K-L, H, S, M, and G represent halo measurements by Kerr-Lawson (*15*), Henderson (*1, 6, 7*), Schilling (*9*), Mahadevan (*10*), and Gentry. Subscripts L, M, and D indicate light, medium (dose 10 to 20 times coloration threshold), and dark (dose about 50 times coloration threshold) induced bands; L→D and L→M indicate light to dark and light to medium; these were visually determined. Gentry's measurements were made with a filar micrometer readable to 0.07 μm. The estimated overall uncertainty was ±0.3 μm. Other abbreviations: N.M., not measured; N.R., not resolved; N.P., not present.

Coloration band size (μm)						U halo radius (μm)						Po halo radius (μm) in									
Biotite			Fluorite	Cordierite	E (Mev)	Nuclide	Biotite			Fluorite		Cordierite	Biotite						Fluorite		
													^{210}Po		^{214}Po		^{218}Po		^{210}Po	^{218}Po	
1. G_L	2. G_M	3. G_D	4. G	5. G	6.	7.	8. K-L	9. H	10. G	11. S	12. G	13. M	14. H	15. $G_{L\to D}$	16. H	17. $G_{L\to M}$	18. H	19. G_M	20. G	21. G
13.4	13.8	14.2	14.1	16.2	←4.2	^{238}U→	12.3	12.7	12.2→13.0	14.0	14.2	16	N.P.	N.P.	N.P.	N.P.	N.P.	N.P.	N.P.	N.P.	N.P.
N.M.	16.7	N.M.	17.3	19.2	←4.77	^{226}Ra→	15.4	15.3	14.8→15.8	16.9	17.1	19	N.P.	N.P.	N.P.	N.P.	N.P.	N.P.	N.P.	N.P.	N.P.
N.M.	N.M.	N.M.	N.M.	N.M.	←4.66	^{230}Th→	N.R.	N.R.	N.R.	15.8	N.R.	N.R.	N.P.	N.P.	N.P.	N.P.	N.P.	N.P.	N.P.	N.P.	N.P.
N.M.	16.7	N.M.	17.3	19.2	←4.78	^{234}U→	15.4	15.3	14.8→15.8	16.9	17.1	19	N.P.	N.P.	N.P.	N.P.	N.P.	N.P.	N.P.	N.P.	N.P.
N.M.	19.3	20.0	19.6	22.5	←5.3	^{210}Po→	N.R.	N.R.	N.R.	19.3	19.5	N.R.	19.8	18.3→19.9	20.0	18.1→19.1	19.9	19.3	19.8	19.8	19.8
N.M.	20.5	21.1	N.M.	N.M.	←5.49	^{222}Rn→	18.6	19.2	18.1→19.0	20.5	20.5	23.5	N.P.	N.P.	N.P.	N.P.	N.P.	N.P.	N.P.	N.P.	N.P.
N.M.	23.0	23.9	23.6	26.7	←6.0	^{218}Po→	22.0	23.0	21.5→22.7	23.5	23.5	26.5	N.P.	N.P.	N.P.	N.P.	24.0	23.3	N.P.	N.P.	23.7
33.1	33.9	34.4	34.6	38.7	←7.69	^{214}Po→	33.0	34.1	30.8→33.0	34.5	34.7	38.5	N.P.	N.P.	34.5	32.5→33.8	34.0	34.0	N.P.	N.P.	34.9

The coloration extinction boundary is poorly defined near threshold coloration; only a few very light bands in biotite could be reliably measured. Reproducible measurements were obtained in the plateau region (*14*), where variations in band size are minimal. Darker halos in biotite generally have slightly larger radii than lighter halos (*3, 4*). Also, reversal effects in some biotites immediately exterior to the terminus of a halo ring cause apparent diminution of the radius. Therefore, while there are differences between the sizes of medium coloration bands (Table 1, column 2) and the radii of U halos in biotite (Table 1, columns 8, 9, and 10) that could be interpreted in terms of an actual change in E_α and λ (*16*), such differences more likely arise from a combination of dose and reversal effects (*15, 17*), producing slightly diminished radii. Diminution of U halo radii may also result from attenuation of α-particles within the small but relatively dense zircon radiocenters. Even though slight differences between band sizes and U halo radii do exist in biotite, the idealized U halo ring structure (Fig. 1a) compares very well with an actual U halo in biotite (Fig. 1f).

Biotite and fluorite are good halo detectors, but fluorite is superior because the halo rings exhibit more detail, often have smaller radiocenter diameters (< 1 μm), and have almost negligible size variations due to dose effects in the embryonic to normal stages of development. Figure 1g shows an embryonic U halo in fluorite with only the first two rings fully developed; the other rings are barely visible because, due to the inverse square effect, threshold coloration has not been reached. Figure 1h shows a U halo in fluorite in the normal stage of development, when nearly all the rings are visible. This halo closely approximates the idealized U halo in Fig. 1a. Under high magnification even separation of the ^{210}Po and ^{222}Rn rings may be seen. Figure 1i shows another U halo in fluorite, with a ring structure that is clearly visible but not adequate for accurate radius measurements.

In Table 1, columns 4, 11, and 12, the fluorite band sizes agree very well with the U halo radii measured in this mineral by myself and Schilling (*9*). This suggests that the differences between U halo radii and band sizes in biotite are not due to a change in E_α. However, experimental uncertainties in measuring U halo radii preclude establishing the constancy of λ to within 35 percent, and under certain assumptions U halos provide no information at all in this respect (*16*).

While halos with point-like nuclei which show well-defined, normally developed rings (as in Fig. 1h) can be used to determine the E_α's of the radionuclides in the inclusion, there are pitfalls in ascertaining what constitutes a normally developed ring. In contrast to the easily recognizable U halos in fluorite in Fig. 1, g to i, the overexposed fluorite U halo in Fig. 1j shows a diminutive ghost inner ring, which could be mistaken for an actual ^{238}U ring. Figure 1k shows two other partially reversed U halos, one of which shows the diminutive inner ring, while in the other all the inner rings are obliterated. The U halo in Fig. 1l is even more overexposed, and encroaching reversal effects have given rise to another ghost ring just inside the periphery. Figure 1m shows a still more overexposed U halo; in which second-stage reversal effects have produced spurious ghost rings that are unrelated to the terminal α-particle ranges.

Since this association of the halos in Fig. 1, l and m, with U α-decay cannot be easily proved by ring structure analysis alone, I have utilized electron-induced x-ray fluorescence to confirm this identification. Figure 3a shows the prominent Ca x-ray lines of the fluorite matrix (the F lines are below detection threshold) along with some background Ag and Rh lines which are not from the sample, but are produced when backscattered electrons strike a Ag-Rh alloy pole piece in the sample chamber. Figure 3b, the x-ray spectrum of a halo radiocenter typical of the halos in Fig. 1, l and m, clearly shows the x-ray lines due to U (as well as a small amount of Si) in addition to the matrix and background peaks. A more detailed analysis (*18*) reveals that the Uζ line masks a small amount of Pb probably generated by in situ U decay.

The variety of U halos shown in Fig. 1, g to m, establishes two points: (i) only a thorough search will reveal the numerous variations in appearance of U halos, and (ii) unless such a search is made, the existence of halos originating with α-emitters other than ^{238}U or ^{232}Th could easily be overlooked.

So far, three criteria have been used to establish the identity of U halos: (i) close resemblance of actual halos in biotite (Fig. 1f) and fluorite (Fig. 1h) to the idealized ring structure

Fig. 2. Densitometer profiles of the photographic negatives of (a) Fig. 1e, (b) Fig. 1f, (c) the light ^{210}Po halo in Fig. 1n, (d) the medium ^{210}Po halo in Fig. 1n, (e) the dark ^{210}Po halo in Fig. 1n, and (f) Fig. 1p.

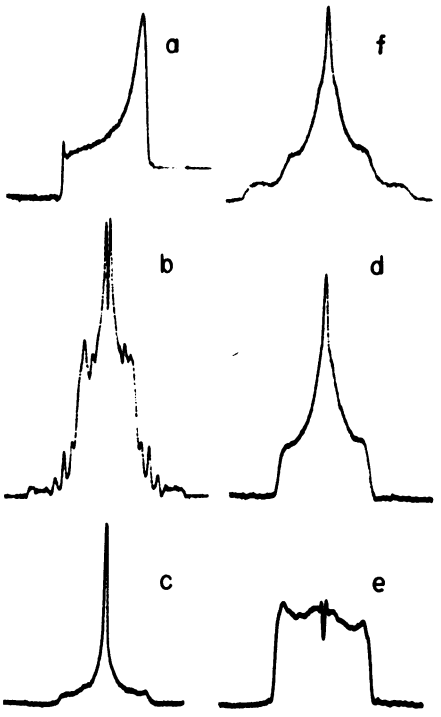

(Fig. 1a), (ii) identification of lines in x-ray fluorescence spectra, and (iii) agreement between U halo radii and equivalent band sizes (very good in fluorite and fair in biotite and cordierite). Using the third criterion (either band sizes or U halo radii), I can determine E_α for a normally developed fluorite halo ring to within ± 0.1 Mev. For biotite halos, U halo radii may form a suitable standard for determining E_α for rings that show reversal or other effects characteristic of U halos in the same sample. If good U halos are not available, and if the halos with variant sizes show well-developed rings without reversal effects, then the band sizes form a suitable standard for E_α determination when coloration intensities of variant halos and band sizes are matched.

Therefore, if halos result from the α-decay of ^{210}Po to ^{206}Pb, their appearance should resemble the idealized schematic (Fig. 1b), and the light and dark halos of this type in biotite should exhibit radius variations consistent with the differences between lower and higher coloration band sizes (Table 1, columns 2, 3, 6, 14, and 15). Further, such halos, whether very light or very dark, should appear without any outer ring structure, as illustrated in Fig. 1n. Compare also the densitometer profiles of the halo negatives of Fig. 1f (the U halo) and Fig. 1n, shown in Fig. 2b and Fig. 2, c to e, respectively. Fig. 1o shows three similar halos in fluorite; here, irrespective of coloration differences, the halo radii are the same and correspond to the E_α of ^{210}Po (Table 1, columns 4, 6, and 20). Accordingly, the halos in Fig. 1, n and o, are designated ^{210}Po halos. (Actually I should emphasize that since not all biotites exhibit the same coloration responses, the radius measurements in Table 1 are strictly valid only for the particular micas I used. I did try to illustrate a range of responses by utilizing four different biotites for the U halo and the three Po halo types.)

By analogy, the moderately developed biotite halo in Fig. 1p shows a marked resemblance to the idealized halo that would form from the sequential α-decay of ^{214}Po and ^{210}Po (see Fig. 1c). Table 1, columns 2, 3, 6, 7, 16, and 17, shows the correspondence of the radii with band sizes. The prominent unmistakable feature of the ^{214}Po halo is the broad annulus separating the inner and outer rings [see the densitometer profile of Fig. 1p shown in Fig. 2f and figures 7 to 9 in (*6*)]. With respect to comments in (*11*) it should be noted that the ^{214}Po halo can easily be distinguished from a U halo.

The last correspondence to be established is the resemblance of the two three-ring halos in biotite (Fig. 1q) and two similar halos in fluorite (Fig. 1r) to the idealized ^{218}Po halo (Fig. 1d) showing the ring structure from the sequential α-decay of ^{218}Po, ^{214}Po, and ^{210}Po. In biotite such halos may appear very light to very dark with radii correspondingly slightly lower and higher (excluding reversal effects) than those measured for medium coloration bands (compare Table 1, columns 2, 3, 18, and 19). Cursory examination of inferior specimens of this halo type could lead to confusion with the U halo, especially in biotite, where ring sizes vary slightly because of dose and other effects. However, good specimens of this type are easily distinguished from U halos, even in biotite. In fluorite, where the ring detail is better, a most important difference between ^{238}U and ^{218}Po halos is delineated, that is, the presence of the ^{222}Rn ring in the U halo (Fig. 1a) in contrast to its absence in the ^{218}Po halo (Fig. 1d). For example, note the slightly wider annulus (3.9 μm) between the ^{210}Po and ^{218}Po rings of the ^{218}Po halo compared to the equivalent annulus (3.0 μm) in the ^{238}U halo (Fig. 1, a, d, h, h', r, and r'). This is evidence that the ^{218}Po halo indeed initiated with ^{218}Po rather than with ^{222}Rn or any other α-decay precursor in the U chain. As further proof, Table 1 (columns 4, 11, 12, and 21) shows that the ^{218}Po halo radii agree very well with equivalent band sizes and U halo radii in this mineral. Additional Po halo types also exist (*3*) but are quite rare. [As yet I have found no halos at all in meteorites or lunar rocks (*19*)].

The preceding discussion has shown

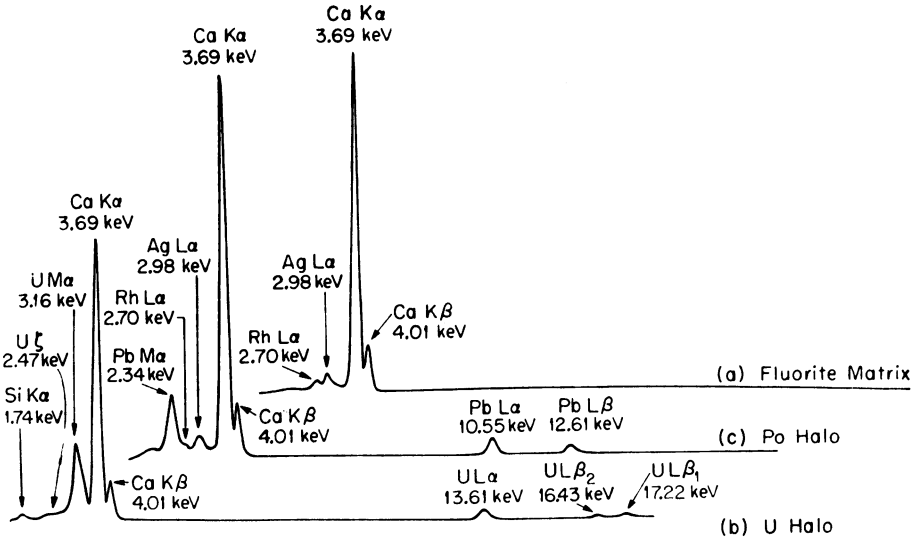

Fig. 3. Scanning electron microscope–x-ray fluorescence spectra of (a) the fluorite (CaF_2) matrix, (b) a U halo radiocenter in fluorite characteristic of Fig. 1, l and m, and (c) a ^{218}Po halo radiocenter in fluorite characteristic of Fig. 1r.

that Po halos can be positively identified by ring structure studies alone. That x-ray fluorescence analyses also provide quite convincing evidence is seen in Fig. 3c, where I show for the first time the x-ray spectra of a Po halo radiocenter (specifically, a ^{218}Po halo). Comparison of Fig. 3, b and c, reveals that the Pb in the Po halo radiocenter in fluorite did not arise from in situ decay of U. [Longer runs have shown small amounts as Se as well as U in some Po halo radiocenters (*18*).] On the other hand, the presence of Pb is to be expected in a ^{218}Po halo radiocenter because the decay product is ^{206}Pb. That the parent nuclide was ^{218}Po and not a β-decaying isomer precursor (*13, 20*) follows from half-life considerations of the U halo U/Pb ratio (> 10); the proposed isomer, if formed at nucleosynthesis, should now be detectable in Po halo radiocenters. No trace of this isomer has yet been found, and I thus view the isomer hypothesis as untenable.

The x-ray data in Fig. 3c are unambiguous and should remove any doubt that previously reported ^{206}Pb/^{207}Pb mass ratios (*3, 13*) actually are Pb isotope ratios, and in fact represent a new type of Pb derived specifically from Po α-decay. In summary, the combined results of ring structure studies, mass spectrometric analyses, and electron induced x-ray fluorescence present a compelling case for the independent existence of Po halos. The question is, can they be explained by presently accepted cosmological and geological concepts relating to the origin and development of Earth?

ROBERT V. GENTRY

Chemistry Division,
Oak Ridge National Laboratory,
Oak Ridge, Tennessee 37830

References and Notes

1. G. H. Henderson, C. M. Mushkat, D. P. Crawford, *Proc. R. Soc. Lond. Ser. A Math. Phys. Sci.* **158**, 199 (1934); G. H. Henderson and L. G. Turnbull, *ibid.* **145**, 582 (1934); G. H. Henderson and S. Bateson, *ibid.*, p. 573.
2. J. Joly, *ibid.* **217**, 51 (1917); *Nature (Lond.)* **109**, 480 (1920). I have examined Joly's collection and found that he associated certain Po halos with U halos and incorrectly associated the ^{210}Po halo as originating with Rn α-decay.
3. R. V. Gentry, *Science* **173**, 727 (1971).
4. ———, *ibid.* **169**, 670 (1970).
5. ———, *ibid.* **160**, 1228 (1968).
6. G. H. Henderson and F. W. Sparks, *Proc. R. Soc. Lond. Ser. A Math. Phys. Sci.* **173**, 238 (1939).
7. G. H. Henderson, *ibid.*, p. 250. A fourth type attributed to ^{226}Ra α-decay is in error.
8. S. Iimori and J. Yoshimura, *Sci. Pap. Inst. Phys. Chem. Res. Tokyo* **5**, 11 (1926).
9. A. Schilling, *Neues Jahrb. Mineral. Abh.* **53A**, 241 (1926). See translation, *Oak Ridge Natl. Lab. Rep. ORNL-tr-697*. Schilling, as did Joly, erroneously designated ^{210}Po halos as emanation halos. As for explanation of the 14.0-μm, 14.4-μm, and 15.8-μm rings which Schilling attributed to UI, UII, and Io, I can state that one of the rings at 14.0 μm and 14.4 μm is a ghost ring. I also rarely observe a light at about 16 μm, but do not presently associate this ring with ^{230}Th (Io) α-decay.
10. C. Mahadevan, *Indian J. Phys.* **1**, 445 (1927).
11. C. Moazed, R. M. Spector, R. F. Ward, *Science* **180**, 1272 (1973).
12. Moazed *et al.* (*11*) stated that because they could not find halos with dimensions matching those of Henderson's type B halo (the ^{214}Po halo in my terminology) such halos do not exist; however, Henderson gave both measurements and photographic evidence (*6*, figure 4, facing p. 242). They then inferred that a different halo (a U halo) must be the equivalent of the type B halo, although the radii of the inner ring of Henderson's type B halo and the outer second ring of their halo were significantly different (20 compared to 22.3 μm). They concluded that all Po halos are only U halos, without having U halos with normal ring structure available for comparison. I showed (*5*) that Po halos and U halos are distinguished by the number of fossil fission tracks after etching; that is, few, if any, compared to a cluster of 20 to 100 tracks. I also showed that the threshold coloration dose is directly obtainable by converting a U halo fossil fission-track count (20 to 100) to the number of emitted α-particles by using the ^{238}U branching ratio, λ_α/λ_f; this contradicts the supposition that such data are unknown to two orders of magnitude. Ion probe analyses of U halos show that a high U isotopic ratio can not be responsible for a small induced fission-track count. Furthermore, contrary to a statement by Moazed *et al.*, Henderson was able to distinguish reliably between his type B and type C halos (*6*, pp. 246–248).
13. R. V. Gentry, S. S. Cristy, J. F. McLaughlin, J. A. McHugh, *Nature (Lond.)* **244**, 282 (1973).
14. The irradiated biotite samples were cleaved in about 5-μm sections for microscopic examination. The coloration threshold (CT) for 30-μm biotite sections varied from 3×10^{13} to 6×10^{13} ^{4}He ions per square centimeter. Band sizes monotonically increased with dose to about 100 CT but were reproducible in a plateau region around 10 to 20 CT. Because band sizes were unpredictable at high beam intensities it was necessary to use beams of only about 10 na/mm^2.
15. D. E. Kerr-Lawson, *Univ. Toronto Stud. Geol. Ser. No. 27* (1928), p. 15.
16. From α-decay theory, $d\lambda/\lambda \simeq (3/2)(ZR)^{1/2}\,(dR/R) + (2Z/E^{1/2})\,(dE/E)$, where Z is the atomic number, R is the nuclear radius in 10^{-15} m, and E ($= E_\alpha$) is the α-decay energy in million electron volts. A particle of mass m and charge z has a range r (halo radius), given by the expression $r = \text{constant} \times E^2/mz^2$. Then $d\lambda/\lambda \simeq 43(dR/R) + 46(dr/r)$. If the difference between the halo radius and the coloration band size at 4.2 Mev is real, then $\Delta r = -0.4$ μm and $d\lambda/\lambda \simeq 46(-0.4/13) = -1.4$. Since the minimum uncertainty in making comparative range measurements is $\Delta r = 0.1$ μm, it is actually impossible to establish the constancy of λ (for ^{238}U) from radio-halo data any better than $d\lambda/\lambda \simeq 46(0.1/13) = 0.35$. Also, if $dE/E = 0$ while $dR/R \neq 0$, then $d\lambda/\lambda \neq 0$. In such a case, halos furnish no proof that λ is constant.
17. Some inner ring coloration in Fig. 1f results from other α-emitters in the U decay chain. Fission track analysis shows that the dose of α-particles from ^{238}U is only about 10^{13} per square centimeter, about ten times less than the ^{4}He ion dose for medium coloration.
18. R. V. Gentry, in preparation.
19. ———, in *Proceedings of the Second Lunar Science Conference* (MIT Press, Cambridge, 1971), vol. 1, pp. 167–168.
20. ———, *Annu. Rev. Nucl. Sci.* **23**, 347 (1973).
21. This work was sponsored by the Atomic Energy Commission under contract with Union Carbide Corporation, and by NSF grant GP-29510 to Columbia Union College, Takoma Park, Maryland.

2 July 1973; revised 26 December 1973

γ-Glutamyl Transpeptidase in Brain Capillaries: Possible Site of a Blood-Brain Barrier for Amino Acids

Abstract. *A fraction containing capillaries and rich in γ-glutamyl transpeptidase was isolated from homogenates of bovine brain cortex by density gradient centrifugation. The enzyme was localized in the endothelial cells by a histochemical procedure. γ-Glutamyl transpeptidase may function in the transfer of some amino acids across the blood-brain barrier.*

γ-Glutamyl transpeptidase catalyzes transfer of the γ-glutamyl residue of glutathione to amino acids according to the following reaction (*1*)

Glutathione + amino acid ⇆
γ-glutamyl amino acid + cysteinylglycine

It was proposed that this reaction, which makes the degradation of glutathione dependent on amino acids, functions in amino acid transport (*2*).

The hypothesis is supported by the finding that γ-glutamyl transpeptidase is associated with cell membranes, especially in those cells where a high rate of amino acid transport is anticipated. Thus, histochemical studies have shown that the enzyme is heavily concentrated in the brush border of the proximal convoluted tubules of the kidney, the apical portion of the intestinal epithelium (*2, 3*), the choroid plexus, and brain capillaries (*4*). The reaction catalyzed by γ-glutamyl transpeptidase was later integrated into the γ-glutamyl cycle (*5*), proposed as a system for amino acid transport. After the amino acid is converted to its γ-glutamyl derivative by γ-glutamyl transpeptidase at or near the cell surface, a translocation step occurs bringing the γ-glutamyl amino acid into the cell (*5*). The amino acid is then released through the action of γ-glutamyl cyclotransferase (*6*) with the concomitant formation of L-pyrrolidonecarboxylic acid (*7*). Conversion of pyrrolidonecarboxylic acid to glutamate (*8*) and synthesis of glutathione complete the cycle. Evidence for the participation of the γ-glutamyl cycle in amino acid transport has been reviewed (*5, 9–11*).

γ-Glutamyl transpeptidase was de-